

Impacts of permafrost degradation on a stream in Taylor Valley, Antarctica



Zachary Sudman^{a,*}, Michael N. Gooseff^b, Andrew G. Fountain^c, Joseph S. Levy^d, Maciej K. Obryk^c, David Van Horn^e

^a 850 Baum Street, Unit D, Fort Collins, CO 80524, USA

^b Institute of Arctic and Alpine Research, University of Colorado, Boulder, CO 80309, USA

^c Department of Geology, Portland State University, Portland, OR 97210, USA

^d University of Texas Institute for Geophysics, Jackson School of Geosciences, University of Texas at Austin, Austin, TX 78712, USA

^e Department of Biology, University of New Mexico, Albuquerque, NM 87131, USA

ARTICLE INFO

Article history:

Received 21 September 2016

Received in revised form 17 February 2017

Accepted 17 February 2017

Available online 20 February 2017

Keywords:

Thermokarst

Antarctica

McMurdo Dry Valleys

Stream bed sediment composition

ABSTRACT

The McMurdo Dry Valleys (MDV) of Antarctica are an ice-free landscape that supports a complex, microbially dominated ecosystem despite a severely arid, cold environment (<5 cm water equivalent/y, −18 °C mean annual air temperature). Recent observations of permafrost degradation in the coastal zones of the MDV suggest that this region is nearing a threshold of rapid landscape change. In 2012, substantial thermokarst development was observed along several kilometers of the west branch of Crescent Stream in Taylor Valley mostly in the form of bank failures, whereas the adjacent east branch was unaffected. The objective of this study was to quantify the changes to the stream banks of the west branch of Crescent Stream and to determine the impacts on the composition of the stream bed material. Three annually repeated terrestrial LiDAR scans were compared to determine the rates of ground surface change caused by thermokarst formation on the stream bank. The areal extent of the thermokarst was shown to be decreasing; however, the average vertical rate of retreat remained constant. Field measurements of bed materials indicated that the west branch and the reach downstream of the confluence (of east and west branches) consistently contained more fines than the unaffected east branch. This suggests that the finer bed material is a result of the thermokarst development on the west branch. These finer bed material compositions are likely to increase the mobility of the bed material, which will have implications for stream morphology, stream algal mat communities, and downstream aquatic ecosystems.

© 2017 Elsevier B.V. All rights reserved.

1. Introduction

The McMurdo Dry Valleys (MDV) are considered one of the driest, coldest deserts on Earth with a mean annual air temperature of around −18 °C and with precipitation that falls as snow amounting to 3 to 50 mm water equivalent (Doran et al., 2002; Fountain et al., 2010). In the MDV the surface energy balance has a much stronger influence on stream flow than precipitation (Hoffman et al., 2008; Gooseff et al., 2011). Snowfall on valley floors generally sublimates before making a significant hydrologic contribution (Conovitz et al., 1998). Despite these harsh conditions, microbial life thrives in the soils, streams, lakes, and even on the glaciers.

The streams of the MDV are considered to be morphologically stable based on the widespread presence of armored bed material

(McKnight et al., 1999) and on little direct observation of change over the past 30 years of research activity. Recent observations, however, suggest that the MDV landscape is changing at rates greater than previously documented (Levy et al., 2013; Fountain et al., 2014). Most of these observations have been in locations where permafrost thaw has caused subsidence of the soil structure (i.e., thermokarst). Thermokarst development influences the topography of a landscape, and if it occurs adjacent to a stream, it can disturb downstream aquatic environments. The failure of stream banks can introduce sediment at rates many times greater than pre-disturbance conditions, and can increase suspended sediment and solute concentrations by several orders of magnitude (Bowden et al., 2008; Kokelj et al., 2013; Gooseff et al., 2016).

Most thermokarst research to date comes from the Arctic because it is a major driver of landscape change in that region. Scientists have only recently begun to assess these same processes in Antarctica. Levy et al. (2013) documented retreat rates of a significant thermokarst feature in Garwood Valley on the Garwood River that had wasting rates on

* Corresponding author.

E-mail address: zachary.sudman@gmail.com (Z. Sudman).

the order of 10 times the estimated Holocene rates, suggesting that the rate of thermokarst degradation is increasing in the MDV. Because of anticipated climate warming in the MDV, understanding the impacts of thermokarst on the morphology, hydrology, and ecology of the MDV has become increasingly important.

In January 2012, substantial thermokarst development was discovered throughout the west branch of Crescent Stream (Fryxell Basin, Taylor Valley; Fig. 1). Substantial bank failures introduced large amounts of sediment to the active stream channel and left steep, unweathered banks (Fig. 2). The adjacent east branch of Crescent Stream, however, was entirely unaffected. Site visits each year since 2012 have documented continued bank degradation on the west branch each year; however, the subsequent degradation has been less severe than the initial impacts.

Here we investigate the impacts of thermokarst development on Crescent Stream and the response of the stream over a 3-year period using high-resolution terrestrial LiDAR scans (TLS) and sediment analysis. Specifically, this study addresses two main research objectives: i) At what rate is the thermokarst development eroding the ground surface on the banks of the stream? These rates were determined by comparing repeat, annual terrestrial LiDAR scans of the impacted area to detect changes in the ground surface elevation. ii) What impacts has the thermokarst activity had on the composition of the bed material of the stream? We conducted sediment size analysis of instream and near-stream sediments to determine whether introduced material was having a significant impact on the bed sediment composition. We then compared the bed material sediment size to the calculated critical unit stream power to estimate potential for stream bed material mobilization. These analyses will help provide understanding of the response of Crescent Stream to future changes of polar streams in response to a warming climate.

2. Site description

Crescent Stream, Taylor Valley, Antarctica ($77^{\circ}37'8.6''\text{S}$, $163^{\circ}11'4.1''\text{E}$) is an ephemeral stream that begins to flow in mid-December and ceases to flow in late January. This range is variable, however, and is dependent on the weather patterns during each flow season. The solar aspect of the glaciers is the primary control on stream flow in the MDV because the glacial runoff is the primary source of water contributing to the stream (>95%). This hydrologic control causes significant fluctuation in stream flow throughout the day based on the position of the sun and topographic relief (Conovitz et al., 1998). The hydrologic variability is not only limited to diurnal cycles, these streams have also been found to have high interannual variation in stream flow, with some annual peak stream flows shown to vary by five times from year to year (McKnight et al., 1999).

Crescent Stream has two branches (east and west) that converge about 500 m upstream of where Crescent Stream discharges into Lake Fryxell (Fig. 1). A stream gage (established in 1990) is located downstream of the confluence of both branches; therefore, estimating the stream flow for each branch was difficult. Field observations from the 2014/2015 season showed similar flows on each branch at the same time; thus, in assessments of flow for each branch, the gage flow was halved as an estimate of the flow in each branch.

Crescent Stream supports complex microbial mat communities composed of cyanobacteria, chemotrophic bacteria, and diatoms (McKnight et al., 1999; Stanish et al., 2013). Throughout the MDV streams, algal abundance has been found to be greatest in stable stream reaches with stone pavements or channel bed armoring (McKnight et al., 1999); whereas growth is limited in unstable, sandy, depositional reaches near the outlets of lakes (Alger et al., 1997). Therefore, understanding the composition and the mobility of stream bed material in

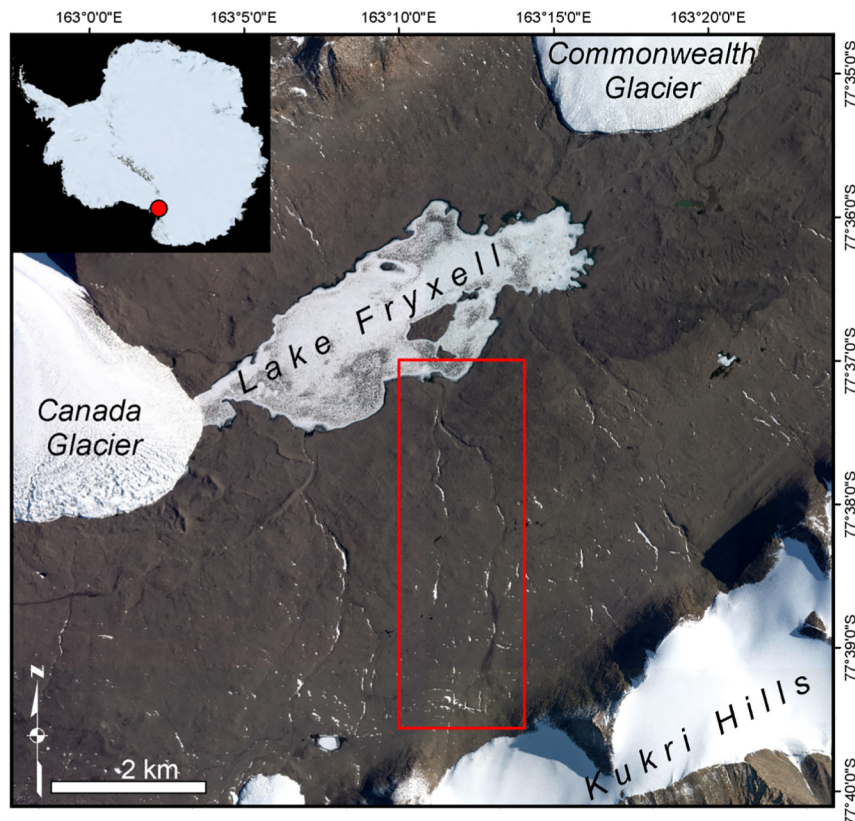


Fig. 1. The Lake Fryxell Basin in eastern Taylor Valley, Antarctica. The red box highlights the east and west branches of Crescent Stream (image data courtesy of Polar Geospatial Center). (For interpretation of the references to color in this figure legend, the reader is referred to the web version of this article.)

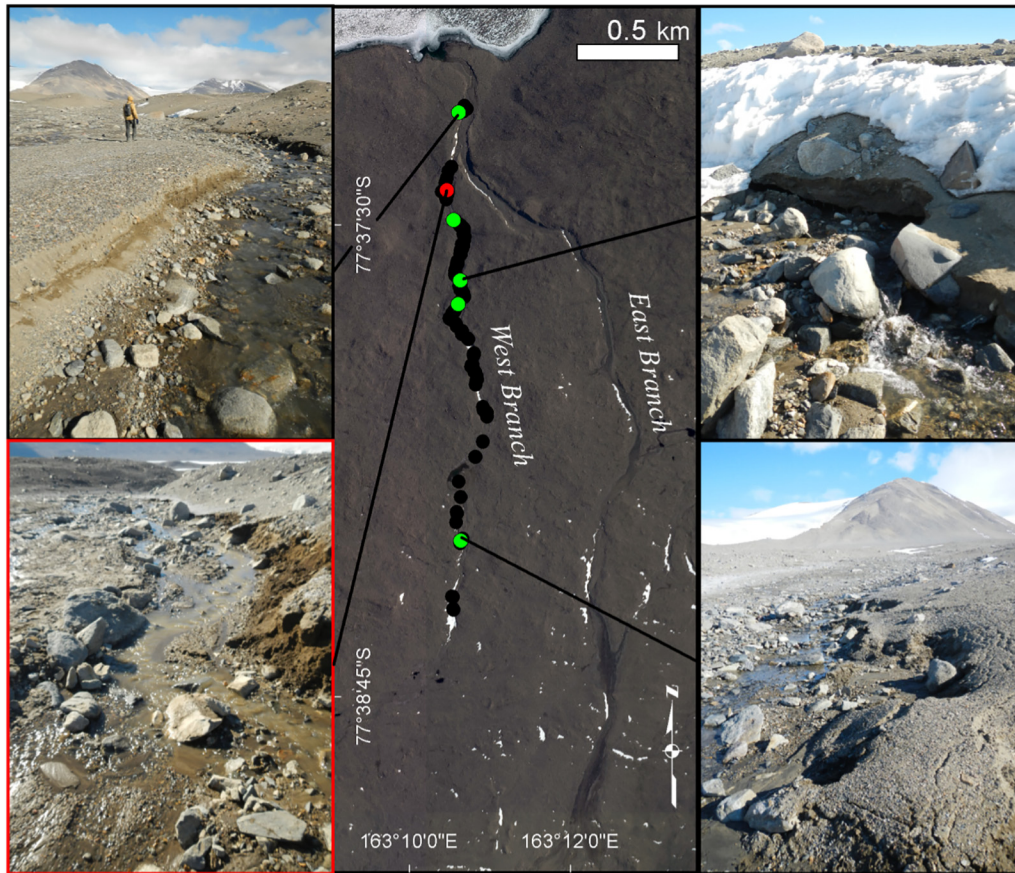


Fig. 2. Images of thermokarst impacts on the west branch of Crescent Stream taken upon discovery in January 2012. Black dots represent locations where impacts were identified in 2012, and the green dots show locations of selected example photographs that illustrate thermokarst subsidence along the banks. The red dot highlights the location of the most substantial thermokarst impact where the terrestrial LiDAR was collected. (For interpretation of the references to color in this figure legend, the reader is referred to the web version of this article.)

the MDV is important because of the influence of these properties on endemic stream communities.

3. Methods

3.1. Terrestrial LiDAR scan (TLS) data collection and processing

Thermokarst activity was discovered on the west branch of Crescent Stream in January 2012; the most heavily impacted area was documented with terrestrial LiDAR scanning, performed by UNAVCO using a Riegel VZ-400. Scans were collected in 2013 and 2014 in the same location to capture the rate of ground surface change that occurred since the initial impacts. No high-resolution survey data are available of the thermokarst impacted area before January 2012. The most substantial changes to the ground surface likely went undocumented. Differences between the new TLS scans and the existing 2001 2-m DEM of Taylor Valley were calculated; however, the 2-m resolution was too low to detect any true changes. The TLS data was processed by UNAVCO using RiSCAN Pro software. The latitude and longitude of each point was converted into the Universal Transverse Mercator 58 South coordinate system, and elevation values were computed in the World Geodetic System 1984 vertical datum.

To accurately compare the LiDAR scans, the resulting point clouds were registered to each other to reduce the minor errors introduced by instrument error, GPS error, and georeferencing errors. The point clouds were registered to each other using a tool available in CloudCompare (Girardeau-Montaut, 2014), an open source point cloud management software. The tool utilizes the *Iterative Closest Point* algorithm (Besl and McKay, 1992).

The point clouds were converted to digital elevation models (DEM) using natural neighbor interpolation with a 1-cm by 1-cm grid cell size resolution. The DEM differencing analysis was performed using the Geomorphic Change Detection 6.1.7 (GCD) software plugin for ArcMap (Wheaton, 2015). For original GCD algorithm details see Wheaton et al. (2009). The result is a DEM of Difference (DoD) with raster cell values that represent the elevation difference between the two survey DEMs. This DoD is used to produce statistics such as retreat rates, volumes, and areas of disturbed landscapes. The inherent uncertainties in survey collection and processing, necessitated the use of a fuzzy inference system to create spatially distributed error surfaces based on the point density of the surveys and on the slope of the terrain. These error surfaces were used to calculate the DoDs with a 95% confidence limit on the calculated differences.

3.2. Sediment sampling

In January of 2015, sediment samples were collected to investigate the effect of thermokarst development on the sediment size distribution of the west branch of Crescent Stream. Three methods were used to characterize the sediment: fine sediment counts, pebble counts, and sediment sieving. The fine sediment counts and the pebble counts (Bunte and Abt, 2001) were performed on reaches throughout both branches of Crescent Stream (see Fig. 3). Reaches were sampled over 50 m measured by tape along one side of the stream following the planform of the stream. Each reach was subsampled at 11 cross sections spaced 5 m apart. The cross sections were sampled at set intervals of 5 or 10 cm to ensure adequate resolution. At each sample interval along the cross section, a long, narrow pin was dropped. For the fine sediment counts, if the pin hit a grain of sediment that was visually identified to be

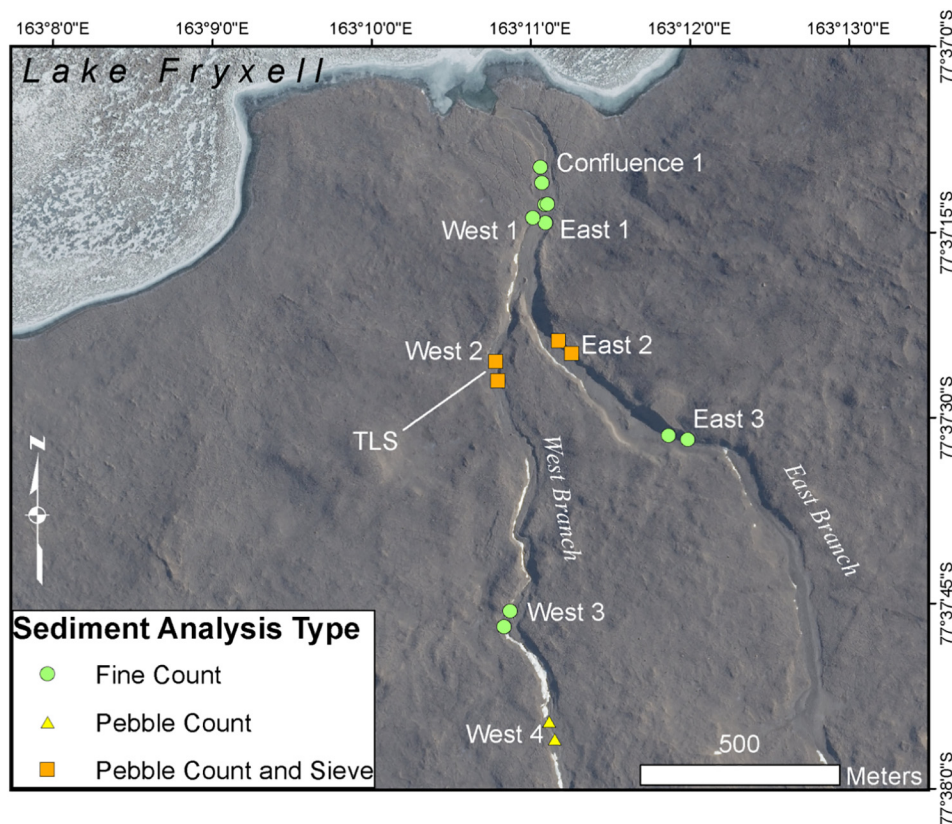


Fig. 3. Map of sample types and locations. Each point represents upstream and downstream limits of sample reach.

<2 mm, then it was classified as fine sediment; otherwise it was classified as coarse sediment. For the pebble count method, the specific grain that was struck by the pin was measured with calipers to determine the diameter of its intermediate axis.

Samples for sieve analysis were collected at two of the sampling reaches: East 2 and West 2 (Fig. 3). The reach on the west branch was chosen because it is located in the midst of the most significant thermokarst activity and was covered by the TLS acquisition. The reach on the east branch was chosen because it was located at a similar distance upstream with a slope similar to the reach on the west branch. Each reach was subsampled at five cross sections each spaced 10 m apart (i.e., every other cross section of the set described above). At each cross section, three characteristic areas of the surface material were visually defined: within the wetted stream channel, locations of fine material and coarse material were defined; and outside the channel, one location of the bank material was defined. Within each characteristic area, two sediment samples were taken: one sample from surface to 2 cm depth and the other from 2 to 8 cm depth. The average sample was around 80 g. The samples were baked in a lab oven at 50 °C for 24 h to ensure all water was evaporated from the samples. The sieve set was comprised of the following sizes: 0, 0.25, 0.5, 1, 2, 3, 4, 6.3, 12.7, and 25.4 mm. This sieve setup was designed to follow the 0.5 phi unit spacing as close as possible; however, it was largely dictated by which sieves were available for use. Before sieving, each individual sieve was weighed. The dried sediment was poured into the sieve set, and the sieve set was shaken using an automated sieve shaker for 1 min. The sieves were individually removed, weighed, and recorded. The mass of the empty sieve was subtracted from the mass of the sieve plus the retained sediment, resulting in the mass of the retained sediment.

3.3. Critical stream power

We sought to estimate the ability of the stream to mobilize sediment within the channel. Because of the low flows experienced in the 2014–

2015 season, little hydraulic data was collected inhibiting implementation of hydraulic and sediment transport models. Stream power was used as a metric to investigate sediment mobilization capabilities while using only gross channel parameters. The unit stream power (ω) is defined as

$$\omega = \rho g Q S / w \quad (1)$$

where Q denotes the flow rate, ρ represents the density of water, g is the acceleration of gravity, S denotes the slope of the channel, and w represents the channel width. This equation represents the mean value of stream power per unit bed area.

Bedload transport in gravel-bedded rivers occurs at a very low rate until a threshold flow rate is reached. After this threshold, transport rates increase nonlinearly. Knowledge of this threshold value is useful in addressing the transport capacity of gravel-bedded rivers. Bagnold (1980) proposed a formula to calculate the critical unit stream power necessary to transport a bed described by a characteristic particle size D . This equation does not, however, distinguish between the grain size being transported and the grain size responsible for bed roughness or account for hiding effects on the mobility of particles. This equation also requires knowledge of the flow depth. Ferguson (2005) derived a critical stream power equation that addressed these criticisms. Ferguson's (2005) full critical unit stream power equation (Eq. (2)) using the Manning-Strickler relation for flow resistance is used in this analysis:

$$\omega_{ci} = a \rho (\theta_{cb} R g D_b)^{\frac{3}{2}} \left(\frac{\theta_{cb} R}{S} \right)^{\frac{1}{6}} \left(\frac{D_i}{D_b} \right)^{5(1-b)/3} \quad (2)$$

where a is a constant from the Manning-Strickler relation with a value of 8.2, D_b is a representative particle diameter (D_{50}) for the bed surface material responsible for the flow resistance, θ_{cb} represents the dimensionless Shields stress for entrainment of particle size D_b , R

denotes the submerged specific gravity, D_i denotes the representative particle size of the bed, and b is the hiding factor with a value between 0 and 1. The representative particle size of a streambed, mobilized by a given stream power, can be solved using Eq. (2). The critical stream power on the left hand side of Eq. (2) can be replaced with Eq. (1) as shown below:

$$\rho g Q S / w = a \rho (\theta_{cb} R g D_b)^{\frac{2}{3}} \left(\frac{\theta_{cb} R}{S} \right)^{\frac{1}{6}} \left(\frac{D_i}{D_b} \right)^{5(1-b)/3} \quad (3)$$

The left hand side of Eq. (3) can be calculated using known measured values of each reach. Only reaches East 2, West 2, and West 4 were used because these were the only reaches with a pebble count to inform the variable D_b in Eq. (3). The slopes of the East 2 and West 2 reaches were determined from 2015 terrestrial LiDAR scans, whereas the slope of West 4 was determined from a 2001 aerial 2-m resolution LiDAR scan of Taylor Valley (Schenk et al., 2004). The thalweg of the stream was extracted and a best fit line was applied to each reach, the slope of that line was taken as the average slope of the reach. The average width of each reach was calculated as the average width of the 11 cross sections within each reach.

A flow duration curve (FDC) was developed for Crescent Stream (Fig. 4) from historic stream gauge data to inform the flow variable in Eq. (3). Crescent Stream has been gaged at 15-min intervals since 1990, and the data were available up to 2013 at the time of this study (www.mcmlter.org). The flow record is fairly complete; however, gaps in the data are present, specifically after the gage was inundated with sediment in January 2012 coincident with the thermokarst activity. Nevertheless, over 41,000 fair to high quality (as noted in the data set) recorded discharges were used for analysis (McKnight, 2014). The only stream gage that exists on Crescent Stream measures the total flow downstream of the confluence of the two branches. Therefore, two FDCs were determined for each branch by assuming either half flow (equal flow contribution from each branch) or total flow (an end-member scenario where all gaged flow comes from one branch).

To solve for the critical unit stream power, each percentile of flow along the FDC was used in the left hand side of Eq. (3) along with the slope of the reach of interest and average width to create a distribution of stream powers with estimated probabilities of occurrence. The

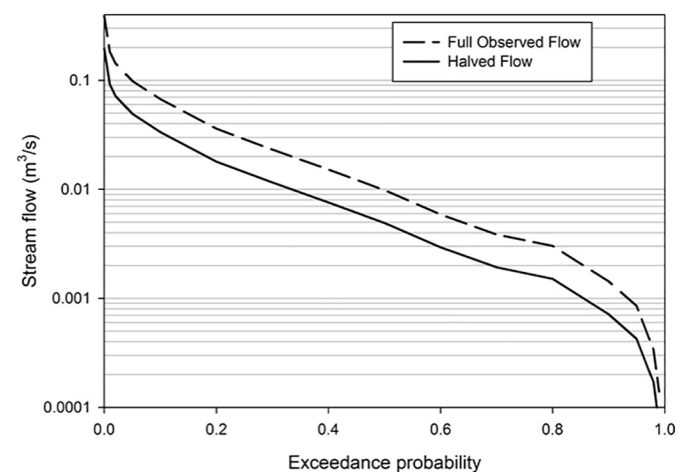


Fig. 4. Flow duration curve of Crescent Stream gage downstream of confluence. Each branch was not gaged individually, so the total gaged flow was halved to estimate what each branch might see (solid line). The actual gaged flow is also shown (dashed line) to represent a maximum end member for the potential flow each branch could see. This flow duration curve was calculated using only flows that were rated *good* or *fair* as noted in the data set. We should note that this is an ephemeral stream and that all zero flow measurements were thrown out.

known values of the right hand side of Eq. (3) were then populated. We assumed that $\rho = 1000 \text{ kg/m}^3$, $g = 9.81 \text{ m/s}^2$, and $R = 1.65$. The critical dimensionless shear stress θ_{cb} was estimated using the measured fractions of sand from Fig. 1 (Wilcock, 1998). The resulting θ_{cb} values were 0.015, 0.029, and 0.037 for West 2, West 4, and East 2 respectively. The constant $a = 8.2$ from the Manning-Strickler relation was used, and $b = 0.7$ was used for the grain hiding factor. The representative surface roughness diameter D_b values used were the D_{50} values calculated from the pebble counts, which were 9.6, 55.1, and 32.5 mm for West 2, West 4, and East 2 respectively. The particle size diameter was estimated using various critical unit stream powers as determined by the FDC.

4. Results

4.1. Rates of ground surface change

Substantial erosion (negative change in ground surface elevation) on the order of 0.5 m was observed from DoDs on the east bank of the west branch for the 2012 to 2013 and the 2013 to 2014 analyses (Fig. 5). Many of the areas of major erosion showed small amounts of deposition (positive change in ground surface elevation) on the order of 0.1 m just downslope of the impacted areas. The total calculated volume of erosion for a 40-m-long reach from 2012 to 2013 was 4.7 m^3 , which was more than double the 1.9 m^3 measured from 2013 to 2014 (Table 1), indicating that the extent of erosion is decreasing with time. The volume of deposition in this reach was 0.29 m^3 from 2012 to 2013 and 0.31 m^3 from 2013 to 2014. Deposition volumes were much lower than erosion volumes, indicating that eroded sediment has either been transported out of the scan area or has been distributed as shallow deposits too small for the analysis to detect. The average depths of erosion for each time period were similar with values of 0.21 and 0.18 m for 2012 to 2013 and 2013 to 2014 respectively. The average deposition

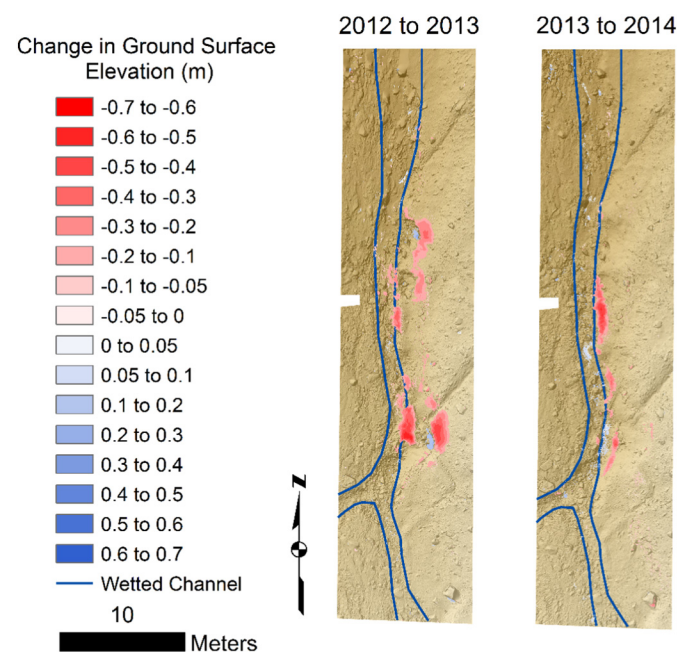


Fig. 5. DEM differencing results of a thermokarst impacted area on the west branch of Crescent Stream. Red coloring indicates areas of measured erosion (decrease in ground surface elevation), and blue coloring indicates areas of measured deposition (increase in ground surface elevation). The location of this reach is indicated in Fig. 3. (For interpretation of the references to color in this figure legend, the reader is referred to the web version of this article.)

Table 1

Quantitative geomorphic change detection results of a reach on the west branch of Crescent Stream (Fig. 5).

	2012–2013	2013–2014
Erosion volume (m ³)	4.68	1.90
Erosion error volume (m ³)	1.36	0.58
Deposition volume (m ³)	0.29	0.31
Deposition error volume (m ³)	0.16	0.41
Area of erosion (m ²)	22.5	10.5
Area of deposition (m ²)	2.81	4.51
Average depth of erosion (m)	0.21	0.18
Average depth of deposition (m)	0.1	0.07

depths for the two years were also very similar with values of 0.1, and 0.07 m respectively.

4.2. Comparison of particle size distribution, fines, and stream power in east and west branches of Crescent Stream

Sediment sieving was used to compare distributions of sediment sizes of the east and west branches as well as to characterize the sediment introduced by the thermokarst formation. The coarse and bank material on both branches had larger surface material when compared to the subsurface material (Fig. 6). The sediment size distribution of the subsurface bank material from the west branch was found to have over 60% of material <2 mm (Fig. 6), indicating that a majority of the sediment introduced to the stream channel as the result of thermokarst

activity was fine material (<2 mm). The sieve results also show a finer distribution for the surface fine and coarse material of the west branch compared to the east branch.

The spatial distribution of fine material and the unit stream power were compared to determine if the thermokarst development has changed the size of the bed material on the west branch. The plot of percent fine versus distance upstream shows the longitudinal distribution of fine sediment throughout the stream network (Fig. 7A). The most upstream reaches of the east and west branches, East 3 and West 4, had very similar average percent fine values of around 21% and standard deviations of about 10%. Moving downstream along the west branch, the percent fine value peaked at the West 3 location, with a value of 52% and a relatively large standard deviation of about 20%. The percentages decreased gradually downstream from 34% at West 2 and then to 31% at West 1 despite lower unit stream powers of 22 and 45 W/m² respectively. On the east branch, the percent fine values remained relatively constant despite a range of unit stream powers from 28 to 43.7 W/m². The average percent fine dipped slightly from 22% at East 3 to 17% at East 2 and then back up to 21% at East 1. The confluence value for the average percent fine value of 35% was larger than all east branch values and similar to the lower two west branch values.

4.3. Does thermokarst development enhance bed material mobilization?

The analyses of the mobilization of bed material (Fig. 8) represent the bed material particle size that would be mobilized given a certain flow, with the solid curve representing half of the observed flow

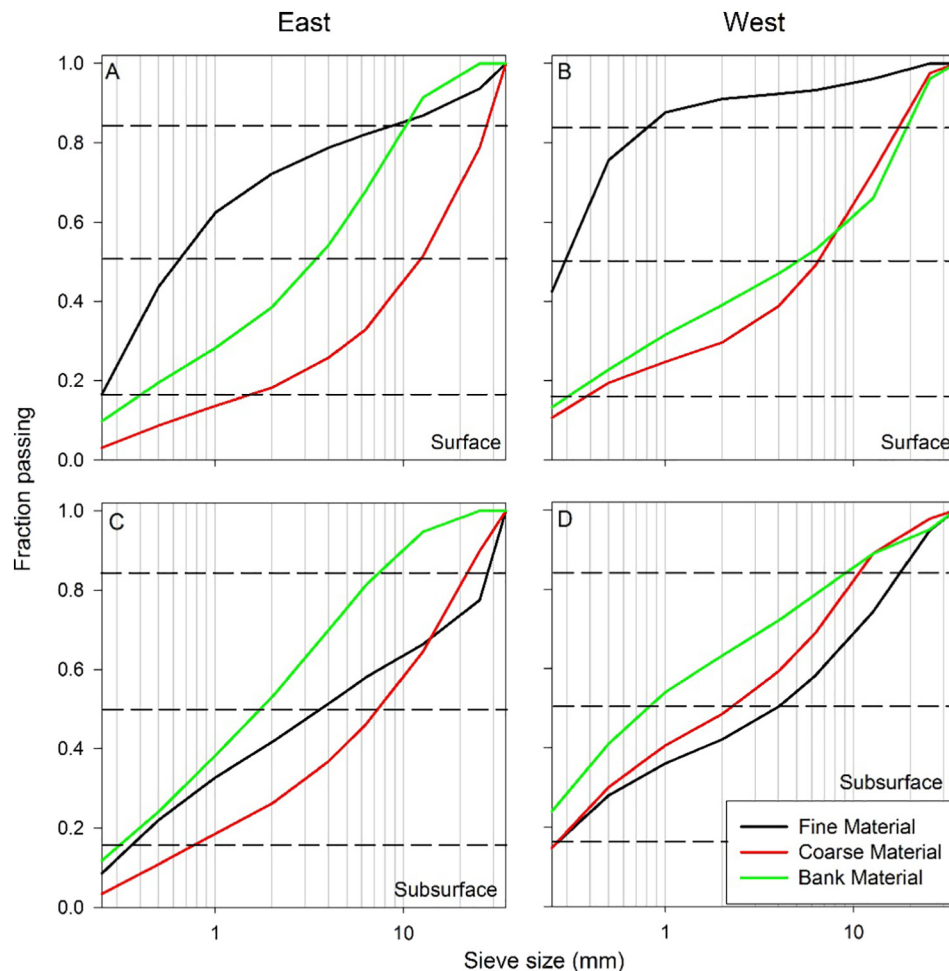


Fig. 6. Sediment size distributions of sieve samples for East 2 and West 2 reaches of Crescent Stream, Taylor Valley, Antarctica. Samples were characterized by reach, surface, or subsurface and by sample location type. (A) east surface material, (B) west surface material, (C) east subsurface material, (D) West subsurface material.

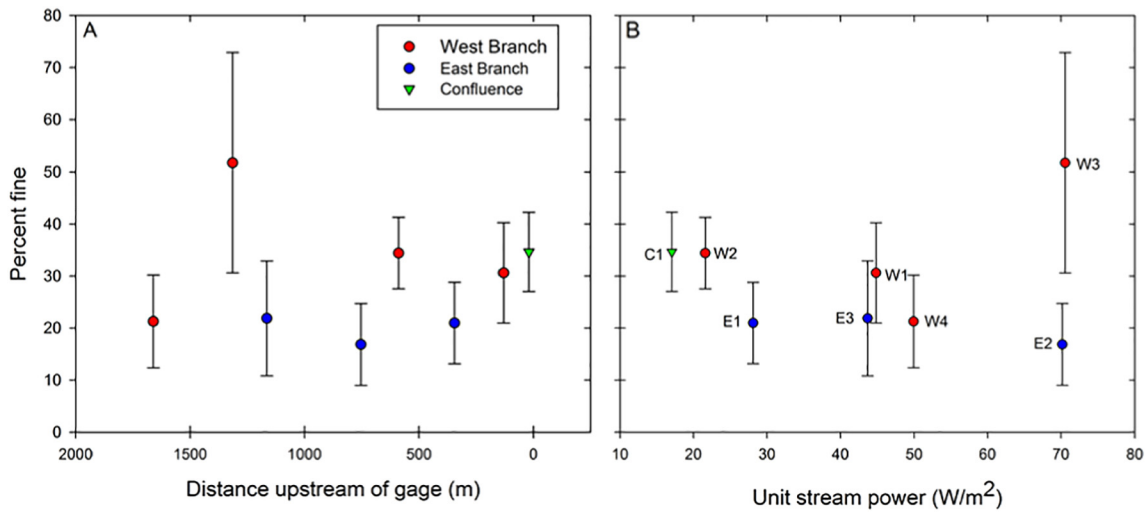


Fig. 7. (A) Percent fine plotted against distance upstream of gage station. (B) Percent fine plotted against unit stream power. Points represent reach averaged percent fine of the 11 cross sections per reach. Error bars represent the standard deviations of the percent fine within each cross section.

(equal flow contribution from each branch) and the dashed curve representing the full observed flow (total flow is experienced by only one branch). The West 4 location had the least capacity to mobilize bed material and had the largest bed material. The location with the greatest bed material transport capacity was West 2, which also had the smallest sediment size distribution. This relationship occurs because a larger fraction of sand (smaller bed material) increases the mobility of the bed material (Wilcock, 1998). These results indicate that the West 2 reach can mobilize its bed material far more frequently than the East 2 and West 4 locations.

5. Discussion

5.1. Rate of ground surface change since initiation of thermokarst

How do the rates of change compare to nearby unaffected areas, and how does the ground surface continue to respond after the initial disturbance in January 2012? To ensure that the measured rates of change on the east bank were substantial compared to nearby rates of change, the opposing unaffected bank (the west bank) was differenced and no change was detected. Without any high resolution survey data of the

site before January 2012, we assumed that the most dramatic changes went undocumented. The geomorphic change that was captured shows a substantial decrease in the volume eroded from 2012 to 2013 to the volume eroded from 2013 to 2014 (Fig. 5, Table 1), suggesting that the rate of erosion caused by thermokarst activity is slowing. However, the average depth of erosion remained constant at about 20 cm. The decrease in the volumetric change was largely because the areal extent of erosion had decreased. The decrease in the area affected, in conjunction with the constant vertical rate of change, suggests that the extent of permafrost susceptible to thaw in the bank is likely decreasing, whereas the drivers of the permafrost thaw appear to be remaining constant.

5.2. Thermokarst impacts on stream sediment

To assess the impacts of the thermokarst development (because of permafrost degradation) on the bed material of the west branch of Crescent Stream, it was necessary to determine the current stream bed material as well as attempt to infer what past bed material composition may have been. The sediment size analysis of the west branch of Crescent Stream was designed to inform the current bed material

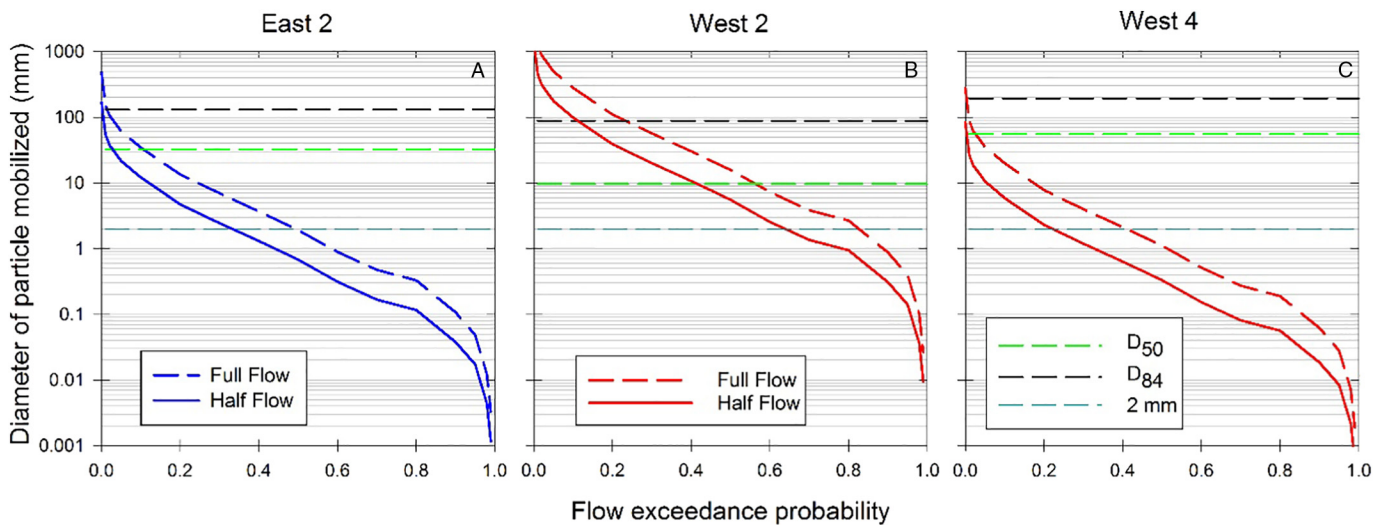


Fig. 8. Bed material particle size mobilization plotted against the flow exceedance probability. Solid curve represents half of observed flow at gage i.e., what one branch would likely experience. Dashed curve represents an end member scenario where all of the flow observed at the gage is flowing through only one of the channels. (A) East 2, (B) West 2, (C) West 4.

composition—as influenced by the thermokarst formation—whereas the analysis of the east branch attempted to determine what the past bed material composition of the west Branch may have been before the thermokarst impacts. The east branch and west branch of Crescent Stream have many similar characteristics including discharge (based on field observations), longitudinal profiles, and substrate (prior to thermokarst formation on west branch). Because of the similarities between the east and west branches of Crescent Stream and because of the relative stability of the east branch, the east branch is a plausible predisturbance reference for the west branch providing a useful baseline condition to compare to the impacted west branch.

To interpret the grain size data, we assumed that the bank material sampled from the west branch (Fig. 6D) was representative of the material that eroded out during thermokarst formation. It is mostly fine material. Looking at the distribution of fine material in Fig. 7A, we find that the thermokarst impacted branch has more fines downstream of the thermokarst impacts than the unaffected branch. We interpret this to indicate that thermokarst erosion in Crescent Stream delivered bank sediments to the channel. Because most tills in Taylor Valley are fine grained (Wagner et al., 2006), we predict that future thermokarst erosion on streams will produce pulses of fine-grained material into stable stream beds that are typically dominated by armored gravels and cobbles.

5.3. Fate of fine sediments introduced to the stream

We expected the input of fine sediment to influence the size distribution of stream bed material. To explore this idea we determined how much fine material was present on the surface of the stream bed for each branch. The average percent fines composition of the West 4 location was very similar to the percent fines of all east reaches and had a similar unit stream power to that of East 3. This indicates that the West 4 branch may also serve as an example of the west branch bed conditions before the thermokarst impacts. The location of West 4 was decided upon because it is located immediately downstream of a long, very low gradient reach. Thermokarst impacts were observed above the West 4 reach in 2012 (Gooseff et al., 2016). The majority of the sediment from those thermokarst impacts, however, is assumed to have been deposited in the upstream low gradient reach, leaving the West 4 reach relatively unaffected. West 4 had the coarsest pebble count measured out of the three west branch reaches that were sampled. This is the result of an absence of sediment loading to this reach combined with a relatively high unit stream power.

Farther downstream, where the thermokarst impacts are more pervasive, the West 3 reach exhibits an unusually high average value of percent fines, accompanied with a large standard deviation. This result is interesting because the West 3 reach has a nearly identical unit stream power as the East 2 reach. However, West 3 has a much higher percentage of fine material when compared to East 2. This suggests that some factor other than stream power is responsible for the increased number of fines on the west branch bed and that the cause is the introduction of fine sediment caused by thermokarst activity.

The West 1 and 2 reaches exhibit a considerable reduction in the average value of percent fines from the West 3 reach, despite lower stream powers. However, the West 1 and 2 locations have a higher average value of percent fines than all of the east branch reaches regardless of unit stream power. These results suggest that upstream introduction of fine sediment from thermokarst activity has caused the composition of the bed material of the west branch to become more fine than the east branch regardless of unit stream power. The confluence also had an average percent fine value larger than the entire east branch. The Confluence 1 location, however, has the lowest stream power; thus, it would be expected to have a higher percentage of fines than other locations. All locations on the east branch had a nearly constant average percent fine value accompanied with relatively small standard deviations. This was a surprising result based on the wide range of stream

powers observed on the east branch. This result suggests that the effect of stream power on the percentage of fines on the bed throughout this branch is minimal.

The pebble counts and the fine sediment counts show that the west branch contains a greater percentage of fine surface material than the east branch, regardless of the varying stream power and upstream conditions. The main difference between these two branches that has the potential to cause this difference in the amount of fine sediment in each branch is the presence of thermokarst throughout the west branch. This result is consistent with other findings of bed material fining after fine-grained sediment pulses (Venditti et al., 2010).

5.4. Comparison of GCD and sediment size analysis

The results of the GCD and the sediment size analysis may appear to be contradictory. The GCD analysis shows very little aggradation in the scan area, while the increased amount of fine sediment found in the west branch could be interpreted as aggradation of fine material on the bed surface. If aggradation of fine sediment did occur within the stream channel, the GCD analysis would have trouble detecting small changes. The aggradation of the bed is likely a small change on the order of a couple of centimeters distributed over a large area, while the average changes the GCD can detect are around 5 cm. Another drawback of the terrestrial LiDAR technology is that it cannot penetrate water. Therefore, the point density is very low wherever water was present within the channel at the time of the scan. Therefore, the GCD analysis more accurately illustrates the changes that have occurred outside of the stream channel, whereas the sediment size analysis explains the changes that have occurred within the stream channel.

5.5. Sediment mobilization capacity of east and west branches of Crescent Stream

The sediment mobilization analysis was intended to assess the extent to which the stream has the ability to transport its own bed material and the sediment introduced by the thermokarst formation. Stream power was used because it allows for the estimation of particle size mobilization using gross channel parameters that are relatively simple to measure. Calculation of unit stream power (Eq. (1)) requires three parameters: slope (S), discharge (Q), and width (w). One of the limitations of this analysis is that the width of the stream at each reach was held constant for different flow rates because of lack of data relating width to flow rate. The East 2 and West 4 locations were similar in their capacity to mobilize bed material. The most severely impacted location, West 2, however, was able to mobilize the available bed material much more readily than the other reaches. The larger fraction of sand in the West 2 transect reduced the dimensionless critical shear stress, resulting in higher bed material mobility (Wilcock, 1998). Fine sediment pulses, similar to what the thermokarst development has produced here, have been found to greatly increase sediment transport rates in gravel-bedded rivers (Venditti et al., 2010). The results of this analysis indicate that the influx of fine sediment promotes the mobilization of the bed material, which will influence the geomorphology and the ecology of the stream, and potentially the receiving closed-basin lake (Gooseff et al., 2016).

5.6. Ecosystem implications of stream bank thermokarst development

The biological communities of Crescent Stream and Lake Fryxell continue to experience environmental changes caused by the thermokarst activity on Crescent Stream as the stream system continues to adjust. The increased bed mobility and finer size of bed material has implications for stream and lake biota. The increased bed mobility causes more sediment to be transported downstream and deposited into Lake Fryxell, which has been shown to hinder primary production in MDV lakes (Foreman et al., 2004). The increased mobility of the bed

material also limits the ability of algae to populate the stream bed (Alger et al., 1997). These potential impacts on the microbial communities of the stream and lake show that as the MDV landscape changes, we can expect to see responses in the downstream ecosystems. It would be interesting to further quantify the ecological impacts that were caused by the thermokarst bank degradation.

6. Conclusion

Ongoing thermokarst development and sediment erosion from the west branch of Crescent Stream has modified bank topography and stream bed sediment distribution over the 2012–2014 observational period. The vertical rates of erosion of ~20 cm/y are constant; however, the areal extent experiencing change has decreased from 24.5 to 10.3 m² from 2012 to 2013 to 2013–2014. The primary impact of the thermokarst development on the west branch of Crescent Stream is an increase in the presence of fine material on the stream bed. The addition of fine material to the west branch of Crescent Stream has increased the mobility of the bed material compared to unaffected reaches. The increased bed mobility has the potential to alter the morphology of the stream and to limit algal growth within the stream. Considering the warming climate and the influence of polar amplification, the initiation of thermokarst features is expected to increase in this region, which will continue to challenge the resiliency of the MDV streams and their dependent biologic communities.

Acknowledgements

This research was funded by NSF grant 1246203. Support was provided by the McMurdo LTER, NSF OPP grant 1115245. The authors wish to acknowledge, Colorado State University for academic funding support, UNAVCO for TLS collection, The Polar Geospatial Center for satellite imagery. The authors would also like to sincerely thank the anonymous reviewers and editor for their help improving this manuscript.

References

- Alger, A.S., McKnight, D.M., Spalding, S.A., Tate, C.M., Shupe, G.H., Welch, K.A., Edwards, R., Andrews, E.D., House, H.R., 1997. *Alger et al.pdf*. Institute of Arctic and Alpine Research, Boulder, CO.
- Bagnold, R.A., 1980. An empirical correlation of bedload transport rates in flumes and natural rivers. *Proc. R. Soc. London A Math. Phys. Eng. Sci.* 372, 453–473.
- Besl, P.J., McKay, N.D., 1992. A method for registration of 3-D shapes. *SPIE* <http://dx.doi.org/10.1117/12.57955>.
- Bowden, W.B., Gooseff, M.N., Balsler, A., Green, A., Peterson, B.J., Bradford, J., 2008. Sediment and nutrient delivery from thermokarst features in the foothills of the North Slope, Alaska: Potential impacts on headwater stream ecosystems. *J. Geophys. Res. Biogeosci.* 113:1–12. <http://dx.doi.org/10.1029/2007JG000470>.
- Bunte, K., Abt, S.R., 2001. Sampling Surface and Subsurface Particle-size Distributions in Wadable Gravel- and Cobble-bed Streams for Analyses in Sediment Transport, Hydraulics, and Streambed Monitoring. Fort Collins, CO.
- Conovitz, P.A., McKnight, D.M., Macdonald, L.H., Fountain, A.G., 1998. Hydrologic processes influencing streamflow variation in Fryxell Basin, Antarctica. *Ecosystem Dynamics in a Polar Desert: The McMurdo Dry Valleys, Antarctica*, pp. 93–108.
- Doran, P.T., McKay, C.P., Clow, G.D., Dana, G.L., Fountain, A.G., Nylen, T., Lyons, W.B., 2002. Valley floor climate observations from the McMurdo dry valleys, Antarctica, 1986–2000. *J. Geophys. Res. Atmos.* 107:1–12. <http://dx.doi.org/10.1029/2001JD002045>.
- Ferguson, R.L., 2005. Estimating critical stream power for bedload transport calculations in gravel-bed rivers. *Geomorphology* 70:33–41. <http://dx.doi.org/10.1016/j.geomorph.2005.03.009>.
- Foreman, C.M., Wolf, C.F., Priscu, J.C., 2004. Impact of episodic warming events on the physical, chemical and biological relationships of lakes in the McMurdo Dry Valleys, Antarctica. *Aquat. Geochem.* 10:239–268. <http://dx.doi.org/10.1007/s10498-004-2261-3>.
- Fountain, A.G., Nylen, T.H., Monaghan, A., Basagic, H.J., Bromwich, D., 2010. Snow in the McMurdo Dry Valleys, Antarctica. *Int. J. Climatol.* 30:633–642. <http://dx.doi.org/10.1002/joc.1933>.
- Fountain, A.G., Levy, J.S., Gooseff, M.N., Van Horn, D., 2014. The McMurdo dry valleys: a landscape on the threshold of change. *Geomorphology* 225:25–35. <http://dx.doi.org/10.1016/j.geomorph.2014.03.044>.
- Girardeau-Montaut, 2014. *Cloud Compare*.
- Gooseff, M.N., McKnight, D.M., Doran, P., Fountain, A.G., Lyons, W.B., 2011. Hydrological connectivity of the landscape of the McMurdo Dry Valleys, Antarctica. *Geogr. Compass* 5:666–681. <http://dx.doi.org/10.1111/j.1749-8198.2011.00445.x>.
- Gooseff, M.N., Van Horn, D., Sudman, Z., McKnight, D.M., Welch, K.A., Lyons, W.B., 2016. Stream biogeochemical and suspended sediment responses to permafrost degradation in stream banks in Taylor Valley, Antarctica. *Biogeosciences* 13 (6):1723–1732. <http://dx.doi.org/10.5194/bg-13-1723-2016>.
- Hoffman, M.J., Fountain, A.G., Liston, G.E., 2008. Surface energy balance and melt thresholds over 11 years at Taylor Glacier, Antarctica. *J. Geophys. Res. Earth Surf.* 113:1–12. <http://dx.doi.org/10.1029/2008JF001029>.
- Kokelj, S.V., Laclelle, D., Lantz, T.C., Tunnicliffe, J., Malone, L., Clark, I.D., Chin, K.S., 2013. Thawing of massive ground ice in mega slumps drives increases in stream sediment and solute flux across a range of watershed scales. *J. Geophys. Res. Earth Surf.* 118: 681–692. <http://dx.doi.org/10.1002/jgrf.20063>.
- Levy, J.S., Fountain, A.G., Dickson, J.L., Head, J.W., Okal, M., Marchant, D.R., Watters, J., 2013. Accelerated thermokarst formation in the McMurdo Dry Valleys, Antarctica. *Sci. Rep.* 3:2269. <http://dx.doi.org/10.1038/srep02269>.
- McKnight, D.M., 2014. *Crescent Stream Gage Measurements*.
- McKnight, D.M., Niyogi, D.K., Alger, A.S., Bombles, A., Conovitz, P.A., Tate, C.M., 1999. Dry Valley streams in Antarctica: ecosystems waiting for water. *Bioscience* 49:985. <http://dx.doi.org/10.2307/1313732>.
- Schenk, T., Csatho, B.M., Ahn, Y., Yoon, T., Shin, W.S., 2004. *DEM Generation from the Antarctic LiDAR Data: Site Report*.
- Stanish, L.F., O'Neill, S.P., Gonzalez, A., Legg, T.M., Knelman, J., McKnight, D.M., Spaulding, S., Nemerget, D.R., 2013. Bacteria and diatom co-occurrence patterns in microbial mats from polar desert streams. *Environ. Microbiol.* 15:1115–1131. <http://dx.doi.org/10.1111/j.1462-2920.2012.02872.x>.
- Venditti, J.G., Dietrich, W.E., Nelson, P.A., Wyzdga, M.A., Fadde, J., Sklar, L., 2010. Effect of sediment pulse grain size on sediment transport rates and bed mobility in gravel bed rivers. *J. Geophys. Res. Earth Surf.* 115. <http://dx.doi.org/10.1029/2009JF001418>.
- Wagner, B., Melles, M., Doran, P.T., Kenig, F., Forman, S.L., Pierau, R., Allen, P., 2006. Glacial and postglacial sedimentation in the Fryxell basin, Taylor Valley, southern Victoria Land, Antarctica. *Palaeogeogr. Palaeoclimatol. Palaeoecol.* 241:320–337. <http://dx.doi.org/10.1016/j.palaeo.2006.04.003>.
- Wheaton, J.M., 2015. *Geomorphologic Change Detection Software*.
- Wheaton, J.M., Brasington, J., Darby, S.E., Sear, D.A., 2009. Accounting for uncertainty in DEMs from repeat topographic surveys: improved sediment budgets. *Earth Surf. Process. Landf.* 156 n/a–n/a. [10.1002/esp.1886](http://dx.doi.org/10.1002/esp.1886).
- Wilcock, P.R., 1998. Two-Fraction Model of Initial Sediment Motion in Gravel-Bed Rivers. *Science* 280 (80):410–412. <http://dx.doi.org/10.1126/science.280.5362.410>.